Research Article | Vol. 11, No. 3 / 1 March 2020 / Biomedical Optics Express 1555
Biomedical Optics EXPRESS

High-speed combined reflectance confocal and moxifloxacin based two-photon microscopy

Bumju Kim,[1] Hoan Le,[1] Byung-ho Oh,[2] and Ki Hean Kim[1,3,*]

[1]*Division of Integrative Biosciences and Biotechnology, Pohang University of Science and Technology, 77 Cheongam-ro, Nam-gu, Pohang, Gyeongbuk 37673, South Korea*
[2]*Department of Dermatology, College of Medicine, Yonsei University, 50-1 Yonsei-ro, Seodaemun-gu, Seoul, 03722, South Korea*
[3]*Department of Mechanical Engineering, Pohang University of Science and Technology, 77 Cheongam-ro, Nam-gu, Pohang, Gyeongbuk 37673, South Korea*
[*]*kiheankim@postech.ac.kr*

Abstract: Reflectance confocal microscopy (RCM) is a non-invasive high-resolution optical imaging technique used in clinical settings as a diagnostic method. However, RCM has limited diagnostic ability by providing non-specific morphological information only based on reflection contrast. Various multimodal imaging techniques have been developed to compensate the limitations of RCM, but multimodal techniques are often slow in imaging speed compared to RCM alone. In this report, we combined RCM with moxifloxacin based two-photon microscopy (TPM) for high-speed multimodal imaging. Moxifloxacin based TPM used clinically compatible moxifloxacin for cell labeling and could do non-invasive cellular imaging at 30 frames/s together with RCM. Performance of the combined microscopy was characterized in the imaging of mouse skin and cornea, *in vivo*. Detail tissue microstructures including cells, extra-cellular matrix (ECM), and vasculature were visualized. The combined microscopy was applied to human skin cancer specimens, and both cells and ECM in the skin cancer and normal skin regions were visualized at high imaging speeds. The combined microscopy can be useful in the clinical applications of RCM by providing multiple contrasts.

1. Introduction

Reflectance confocal microscopy (RCM) is a 3D imaging technique based on light reflection from samples. RCM has been used as a diagnostic method in clinical settings by providing high-resolution cellular images non-invasively [1–7]. In dermatology, RCM has been used for non-invasive detection of skin cancer boundary to guide the surgery of non-melanoma skin cancers [2–5]. In ophthalmology, RCM has been used for non-invasive detection of infecting pathogens in the diagnosis of corneal keratitis and other ocular surface complications [6,7]. However, RCM has limitations in the clinical applications by providing morphological information based on reflection contrast. Reflection contrast is usually not sensitive for detecting small lesions in disease tissues due to the disruption of micro-structures. Even if reflection contrast provides clear visualization, morphological information from RCM may not be specific to detect cells of interest or infecting pathogens. Microstructures of similar morphologies as target pathogens may exist and they may not be distinguished by RCM.

In order to overcome the limitations of RCM, multimodal techniques have been developed to provide additional contrasts or information together with reflection contrast [8–17]. RCM was combined with fluorescence confocal microscopy (FCM) for simultaneous reflection and fluorescence imaging [8–11]. However, the RCM and FCM combination is usually not applicable to human due to the toxicity of exogenous labeling agents used in FCM, unless FCM imaging is based on tissue auto-fluorescence (AF) or FDA approved contrast agents such as fluorescein and indocyanine green (ICG). Two-photon microscopy (TPM), which is another 3D fluorescence

#385763 https://doi.org/10.1364/BOE.385763
Journal © 2020 Received 16 Dec 2019; revised 16 Feb 2020; accepted 17 Feb 2020; published 21 Feb 2020

Biomedical Optics EXPRESS

microscopy based on nonlinear two-photon excitation of fluorophores, was combined with RCM for imaging based on both reflection and AF [12–15,18]. TPM can image cells and extra-cellular matrix (ECM) including collagen in tissues without exogenous labeling by using AF and second harmonic generation (SHG). However, label-free TPM is slow compared to RCM by using weak AF and SHG. Raman spectroscopy was combined with RCM for simultaneous structural imaging and chemical vibrational spectrum measurement [16,17].

Recently, we introduced moxifloxacin as a clinically compatible cell labeling agent for TPM. Moxifloxacin is a 4th generation fluoroquinolone antibiotic used either to treat or to prevent infection in the eye and lung [19]. Pharmacokinetic studies of moxifloxacin showed relatively fast penetration into biological tissues and high intracellular distribution, which are good for tissue labeling [19]. Moxifloxacin has intrinsic florescence, excited at ultraviolet wavelength. Nonlinear two-photon and three-photon excitations of moxifloxacin were demonstrated with near-infrared (NIR) excitation wavelengths from 700nm to 800nm [19–21] and at 1053 nm [22], respectively. With moxifloxacin application, TPM could image approximately 10 times faster than label-free TPM [19]. Moxifloxacin based TPM of various *ex-vivo* skin cancer tissues visualized specific cellular features at a relatively high speed [23]. Moxifloxacin labeled the cell cytoplasm in case of epithelial cells and both the cell cytoplasm and nucleus in case of stromal cells [19]. Moxifloxacin TPM might be able to be used together with RCM for high-speed multimodal imaging.

In this report, we developed a combined reflectance confocal (RC) and moxifloxacin based two-photon (TP) microscopy for multi-contrast high-speed tissue imaging. The combined microscopy was based on high-speed TPM using a resonant scanner and an additional confocal reflection channel. The combined microscopy was characterized and then applied to multi-contrast imaging of the mouse skin and cornea, *in vivo*. Then, the combined microscopy was used to image human skin cancer specimens and the results were compared with the images in the RC mode only and histology.

2. Method

2.1. System configuration

A simplified schematic of the combined microscopy is shown in Fig. 1. The combined microscopy was based on high-speed TPM using a resonant scanner running at 8 KHz, and an additional channel for confocal reflection detection. The system had two fluorescence channels to resolve moxifloxacin fluorescence and SHG, and a reflection channel. The combined microscopy used a Ti-Sapphire laser (Chameleon II, 140fs, Coherent) as the light source for both fluorescence and reflection imaging. The laser beam from the source first passed through a power control unit, consisting of a motorized half wave plate (HWP, 10RP52-4, Newport) and a polarizer (PL, GL5-B, Thorlabs). After the power control unit, the laser beam was expanded by a lens pair (f = 50mm & 100mm) in 4f configuration and passed a beam splitter (50:50), which was installed to collect reflected light from the sample. The transmitted laser beam went to the combination of a resonance scanner and a galvanometer scanner for 2 axis scanning. After the scanner combination, the laser beam was expanded by the combination of a scan lens (f=50mm) and a tube lens (f=200mm). The excitation beam was transmitted through a long-pass dichroic mirror (700LP, Chroma) and went to an objective lens (XLUMPLFN 20x, 1NA, 2mm WD, water immersion, Olympus Inc.). The objective lens focused the excitation laser into the sample. The excitation focus scanned the sample in the transverse plane with the Galvo & Resonant scanner combination. Axial scanning was performed with a piezoelectric objective translator (209SRG&P-725-4CD, PI). Emission light from the sample was collected by the objective lens, reflected on the dichroic mirror, passed through a barrier filter (680SP, Chroma), spectrally split by a dichroic mirror (450SP, Chroma) and emission filters (390nm – 410nm, Thorlabs), and then collected at two photomultiplier tubes (PMTs, H10770A-40, Hamamatsu). The two fluorescence

Biomedical Optics EXPRESS

channels collected moxifloxacin fluorescence and SHG light separately. Signals from the PMTs were fed into transimpedance amplifier (DHPCA-100, Femto) and then a data acquisition board (NI-5734, National Instrument). Reflected light from the sample was also collected by the objective lens and transmitted through the dichroic mirror and the lens pair, reflected on the scanner for de-scanning, and then partially reflected on the beam splitter. De-scanned reflected light was focused by a lens (f = 50mm), transmitted through a pin hole (15μm, Thorlabs), and then collected by a PMT (R5929, Hamamatsu). Signal from the PMT was fed into an amplifier (C6438, Hamamatsu), and then the acquisition board. Signal acquisition in the RC, TPF and SHG channels was performed simultaneously. Laser scanning and data acquisition were controlled by an output board (National Instruments), and Scanimage software (Vidrio Technology).

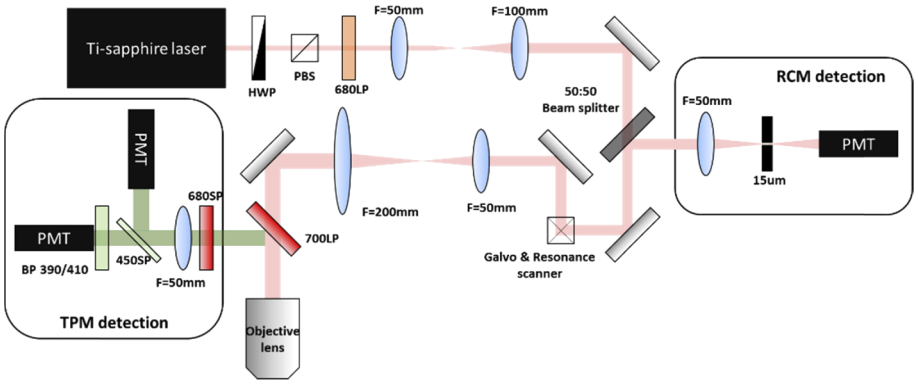

Fig. 1. Schematic of RC and TP combined microscopy

Both RC and moxifloxacin TP images were acquired at 31 frames/s. Both images typically had the field of view (FOV) of 470 μm x 470 μm consisting of 512 × 512 pixels. 3D volumetric images were obtained by acquiring multiple transverse plane images with stepwise axial increment by 1 μm. Excitation wavelength was 790 nm and excitation power was approximately 11 mW. Image resolution was characterized by 3D imaging fluorescent microspheres (0.2 μm in diameter, F8811, Invitrogen) embedded in 2% agarose gel and by analyzing intensity profiles in both the transverse and axial directions. Image resolution was measured as full width at half maximum intensity (FWHM) from the intensity profile. RC imaging showed the image resolution of 0.7 μm and 2.4 μm in the lateral and axial directions respectively. TP imaging showed the image resolution of 0.7 μm and 3.0 μm in the lateral and axial direction respectively. The image resolution in both RC and TP imaging was less than the theoretical one based on the numerical aperture of the objective lens due to the underfilling of excitation laser beam on the back aperture of the objective lens. RC and TP images were post processed in MATLAB (MathWorks) with a block matching 3D filter for de-noising [24].

2.2. Sample preparation

In this study, 8-week old female hairless mice (SKH1-HrHr, ORIENT BIO Inc, Korea) were used. During the imaging, mice were anesthetized by inhaling gas mixture of 1.5%/vol isoflurane (Terrel, Piramal) and medical grade oxygen. A heating plate (Chamlide TR, Live cell Instrument, Korea) was used to maintain the body temperature at 37°C during the anesthesia. Custom-made holders were used for *in vivo* imaging of the mouse cornea and ear to minimize breathing motion during imaging [25]. Moxifloxacin ophthalmic solution (Vigamox, Alcon Laboratories, Fort Worth, US, 12.4 mM) was used to label tissues prior TP imaging. In case of the skin, the stratum corneum was removed via gentle tape stripping before moxifloxacin application, and then drops of moxifloxacin solution were instilled for 20 minutes. In case of the cornea, single drop of

Biomedical Optics EXPRESS

moxifloxacin solution was instilled and then eye lids were closed for 5 minutes. Remaining moxifloxacin on both skin and cornea surface was removed by washing with phosphate buffered solution (PBS). The combined RC and TP imaging was conducted in either 3D or time lapse mode.

Ex-vivo human basal cell carcinoma (BCC) specimens were used to test the feasibility of multi-contrast imaging. Human skin specimens were collected at Severance Hospital of Yonsei University (Seoul, Rep. of Korea) in January 2019. The acquired specimens were imaged in fresh condition within 12 hours after collection. BCC samples were imaged after immersion in moxifloxacin ophthalmic solution for 5 minutes. Remaining moxifloxacin on the sample surface was removed by washing with PBS. BCC diagnosis was histopathologically confirmed. The study protocol was approved by the Institutional Review Board of Yonsei University, Severance Hospital. This study was conducted in compliance with Declaration of Helsinki. Personal information of patient was anonymized and de-identified before analysis.

3. Results

3.1. Combined moxifloxacin TP and RC imaging of the mouse skin, in vivo

The combined microscopy was characterized in the imaging of mouse skin, *in vivo*. Mouse ear skin was imaged in either 3D or single planes, and representative 3D images are shown in Fig. 2. *En-face* moxifloxacin TP and RC images at 6 different depths covering the epidermis and dermis are shown (4μm, 16μm, 24μm, 41μm, 64μm, 105μm deep from the surface). Moxifloxacin TP images were made by combining two-photon fluorescence (TPF) of moxifloxacin and intrinsic SHG in two different colors of green and blue respectively. In the epidermis, epidermal cells appeared both in the TPF and RC channels. Epidermal cells were large and flat in the superficial epidermis (Fig. 2(a)) and small in the basal epidermis (Fig. 2(b)). In the TPF channel, individual cells were resolved with high moxifloxacin fluorescence in the cell cytoplasm and no fluorescence in the cell nucleus. In the RC channel, individual cells were resolved with relatively high reflection on the cell membrane. In the dermis, dermal cells and collagen were shown in the TPF/SHG channel and fibrous ECM structures and vessels were shown in the RC channel (Fig. 2(c, d)) Scattered cells in the dermis were shown in the TPF channel with moxifloxacin labeling, while they were not visible in the RC channel. Cell clusters in the hair follicles were shown in the TPF channel. Collagen in ECM was visualized in the SHG channel. Fibrous ECM structures were clearly visible in the RC channel. Relatively large fibrous structure and collagen content in ECM were visualized by the combination of SHG and RC channel images. Blood vessels were shown in both the RC and TPF/SHG channel (Fig. 2(d, e), red arrows). Blood vessels were clearly identified in the RC channel video (Visualization 1) owing to the temporal change of speckles during imaging associated with blood flow. Blood vessels appeared with relatively strong reflection on the top surface of blood vessels and weak reflection inside in the RC channel. Blood vessels appeared partially in the TPF/SHG channel with moxifloxacin labeling of endothelial cells. Large blood vessels deep inside the skin appeared in the RC channel (Fig. 2(f), red arrows) only, probably because moxifloxacin did not penetrate enough and collagen SHG signal was also very weak at this depth due to the scattering of excitation light. There were other structures which appeared empty in both the RC and TPF/SHG channels (Fig. 2(e), yellow arrows). The structures were much larger than nearby blood vessels and had no reflection and no SHG inside. These empty structures could be lymphatic vessels which were reported in the literature [26,27]. Cellular structure in the epithelium were accessible in both the RC and TPF channel images. In the dermis, cells and collagen were visualized in the TFP/SHG channel and fibrous ECM structure and vessels were visualized in the RC channel. Combination of TPF/SHG and RC channel images clearly visualized microenvironments in the skin by imaging cells, ECM, and blood and lymphatic vessels.

Biomedical Optics EXPRESS

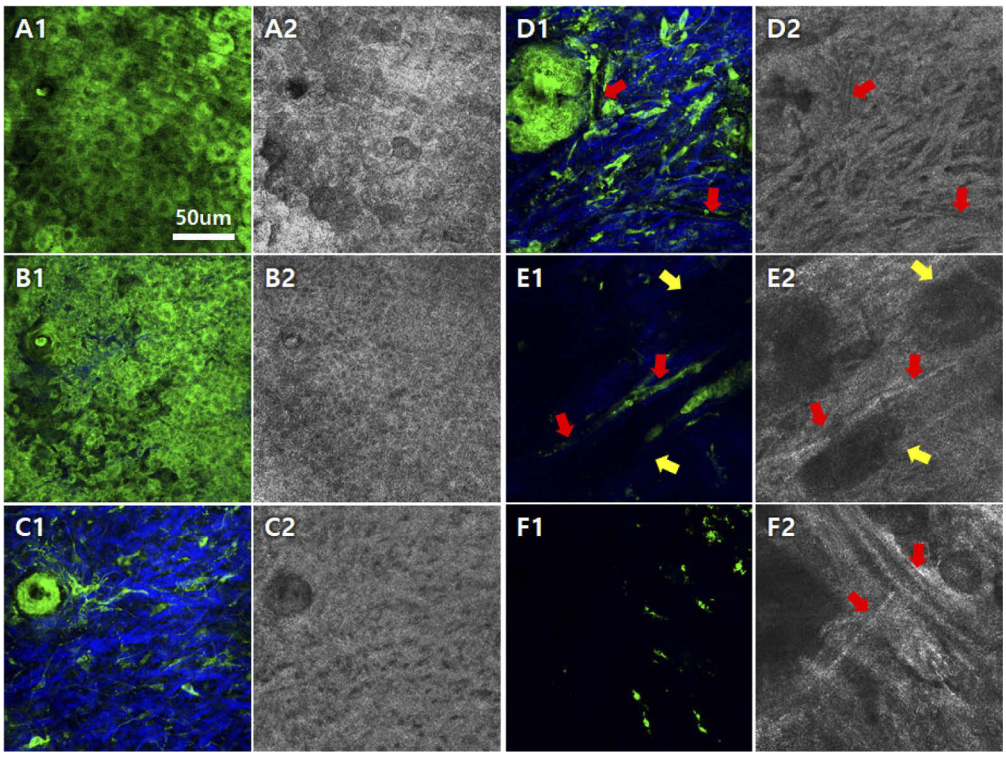

Fig. 2. *In vivo* 3D moxifloxacin TP and RC images of the mouse ear pinna skin (Visualization 1). *En-face* moxifloxacin TP (A1 - F1) and RC (A2 – F2) images at 6 different depths of 4μm, 16μm, 24μm, 41μm, 64μm, 105μm from the skin surface are shown. (A1, 2): the stratum corneum, (B1, 2): the basal layer, (C1, 2 – F1, 2): the dermis at 3 different depths. TP images are color-coded in green and blue scales for moxifloxacin fluorescence and SHG, respectively. RC images are color-coded in gray scale. Blood and lymphatic vessels in the dermis are marked with red and yellow arrowheads, respectively.

3.2. *Combined moxifloxacin TP and RC imaging of the mouse cornea, in vivo*

The cornea is another application field of RCM: non-invasive and early diagnosis of corneal infection by detecting infecting pathogens. The combined microscopy was applied to normal mouse cornea, *in vivo* and results are shown in Fig. 3. Combined moxifloxacin TP and RC images visualized cells and ECM in the epithelium (Fig. 3(a-c)), stroma (Fig. 3(d)), and endothelium (Fig. 3(d)) of the mouse cornea by using different contrasts. *En-face* corneal images in Fig. 3 were flattened to show individual corneal layers from the raw images taken from the curved corneal surface. Some breathing motion appeared as wavy patterns in the flattened images (Fig. 3(a1)). In the epithelium, relatively large and flat cells in the superficial epithelium (Fig. 3(a)) and small cells in the basal epithelium (Fig. 3(b, c)) were shown in both the TPF and RC channels. In the TPF channels, epithelial cells expressed relatively uniform moxifloxacin fluorescence in the cell cytoplasm. Individual cells were resolved with relatively weak fluorescence on the cell boundaries and the intensity variation among cells. In the RC channel, cells were resolved by relatively high reflection on the cell boundaries owing to refractive index mismatch. Cells in the basal epithelium were resolved more clearly compared to those in the superficial epithelium, because cells in the basal epithelium were small and elongated compared to the ones in the superficial epithelium. Sub-basal nerve plexuses were also observed in both the moxifloxacin TP and RC channels, although they appeared clearly in the RC channel owing to high reflection

Biomedical Optics EXPRESS

associated with refractive index mismatch (Fig. 3(c)). In the stroma, cells like keratocytes and nerves and collagen were visualized. Cells appeared in both the TPF and RC channels by expressing moxifloxacin fluorescence and relatively high reflection, and collagen appeared only in the SHG channel (Fig. 3(d)). Cells were visible clearly in the RC channel with relatively high reflection, and nuclei of the cells were visible in the TPF channel. In the endothelium, cells appeared clearly in the RC channel, while did not appeared in the TPF channel probably due to the insufficient moxifloxacin labeling. In the normal mouse cornea, cells in all the corneal layers were clearly visualized in the RC channel and visualized in the TPF channel with additional fluorescence contrast. Collagen in the stroma was visualized in the SHG channel. Although RC contrast was enough to visualize most of cellular structure in the normal cornea, additional contrasts of cells and collagen will be useful for the imaging of diseased turbid corneas.

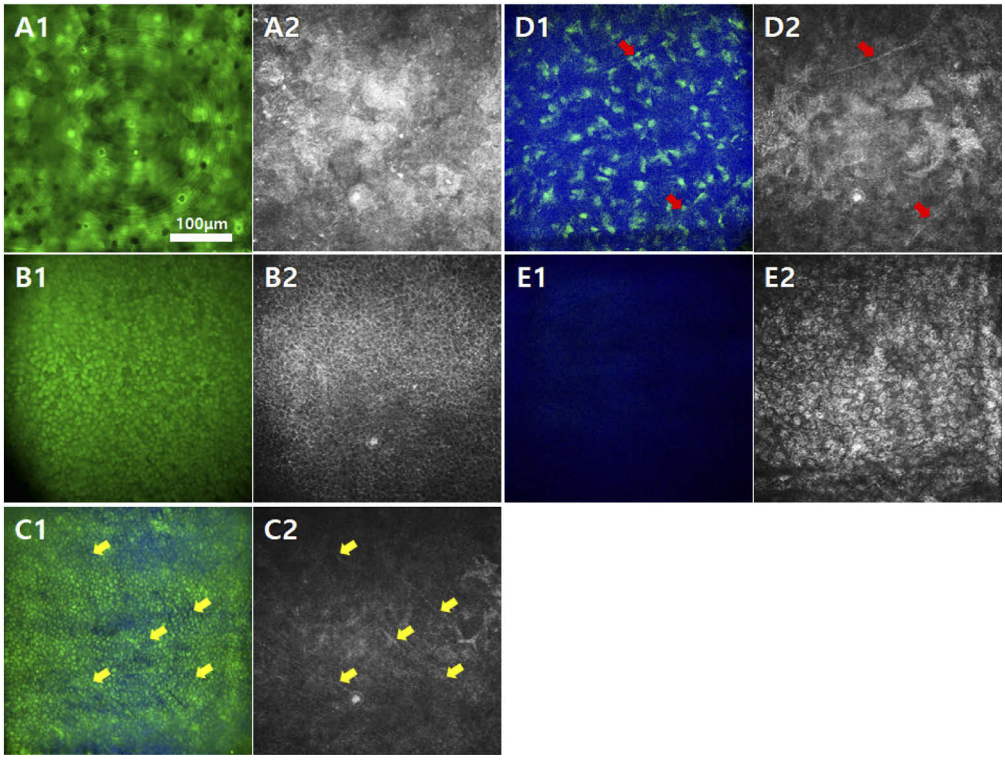

Fig. 3. *In vivo* 3D moxifloxacin TP and RC images of the mouse cornea (Visualization 2). *En-face* moxifloxacin TP (A1 - E1) and RC (A2 – E2) images at 5 different depths of 3μm, 15μm, 20μm, 33μm, 65μm from the surface are shown. (A1 and 2): the superficial epithelium, (B1 and 2): the basal epithelium, (C1 and 2): the sub-basal nerve plexus (yellow arrow), (D1 and 2): the stroma showing nerves (red arrow), (E1 and E2): the endothelium. TP images are color-coded in green and blue scales for moxifloxacin fluorescence and SHG, respectively. RC images are color-coded in gray scale.

3.3. Combined moxifloxacin TP and RC images in the mouse cornea and skin

Images in the moxifloxacin TPF/SHG and RC channels were combined to demonstrate the benefit of multiple contrasts. Combined moxifloxacin TP and RC images of the mouse cornea and skin are presented in Fig. 4. The combined images were made by using different colors for individual contrasts: green, blue and red colors for moxifloxacin TPF, SHG and RC, respectively. In case of the mouse cornea, individual images and a combined image of the corneal stroma

Biomedical Optics EXPRESS

were presented in Fig. 4(a-c). Individual images in the TPF and RC channels showed cells in the corneal stroma such as keratocytes and nerves, but the individual images visualized different features of the cells. Cell nuclei were mainly shown in the TPF channel owing to the variation of moxifloxacin intracellular distribution (Fig. 4(a)). The overall shape of the cells including cell cytoplasm was visualized in the RC channel owing to light reflection from the cell membrane (Fig. 4(b)). Collagen in the corneal stroma was visible in the SHG channel (Fig. 4(a)). The combined image of the corneal stroma showed both the nucleus and cytoplasm of cells in different colors by combining the two individual images. In case of the mouse skin, individual images and a combined image of the skin dermis was presented in Fig. 4(d-f). Individual images in the moxifloxacin TPF/ SHG and RC channels showed different microstructures in the skin dermis. In the moxifloxacin TPF channel, cells including individually distributed dermal cells, cell clusters in the hair follicles (yellow arrowheads), endothelial cells on the wall of blood vessels (white arrowheads), and nerves (purple arrowheads) were visualized (Fig. 4(d)). In the RC channel, the distribution of ECM including fibrous structures and hair follicles were visualized based on the variation of reflection intensity (Fig. 4(e)). Blood flows was visualized in the RC channel owing to temporal intensity fluctuation during image acquisition. The combined image of the skin dermis visualized cells, ECM structures, and blood flow altogether (Fig. 4(f)). Blood flow appeared in high contrast via additional processing of temporal intensity variation. Some blood flow was around the hair follicles, and others were across the dermis. Detail microenvironments in the skin dermis were visualized by the combination of reflection, moxifloxacin TPF, and SHG.

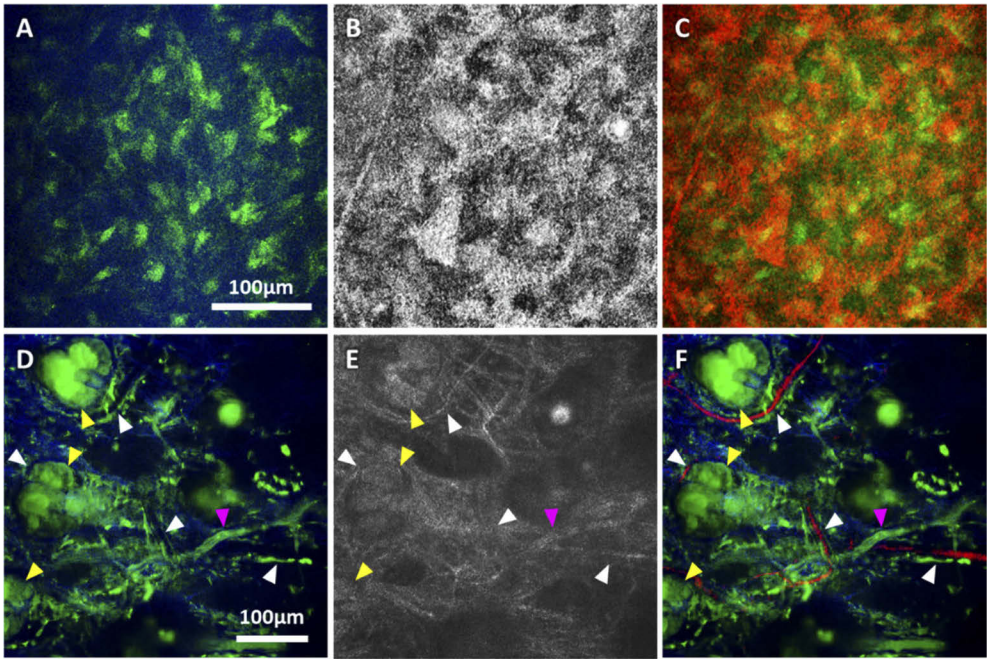

Fig. 4. Combined *en-face* images of the mouse corneal stroma and skin dermis, *in vivo*. (A-C): individual images of the corneal stroma in the moxifloxacin TPF/SHG (A) and RC (B) channels and a combined image (C). In the combined image, the RC channel image was color-coded in red for the enhanced contrast with the TPF/SHG channel image which was color-coded in green and blue. (D-F): individual images of the skin dermis in the moxifloxacin TPF/SHG (D) and RC (E) channels and a combined TPF/SHG and blood flow image (F).

Biomedical Optics EXPRESS

3.4. Combined moxifloxacin TP and RC imaging of the human basal cell carcinoma (BCC), ex vivo

Lastly, the combined microscopy was applied to human skin cancer specimens, and the imaging results of a human basal cancer carcinoma (BCC) specimen are shown in Fig. 5. BCC is the most common skin cancers. BCC specimens were selected as the sample for testing the combined microscopy, because BCC is a skin cancer type with relatively clear cancer-normal tissue boundary and BCC margin detection has been extensively studied by RCM [4,5]. A bright-field image of the BCC specimen and two hematoxylin and eosin (H&E) labeled histological images are shown in Fig. 5(a) and (b-c). The bright-field image showed a partially pigmented skin specimen. Upper side of the specimen including pigmented region was BCC. H&E staining histological images in two different field of views (FOVs) showed cancer cell distribution in the specimen (Fig. 5(b-c)). A large FOV histological image showed BCC in the upper side and some normal skin in the lower side (Fig. 5(b)). A zoomed histological image inside the BCC showed cancer cell nest structures (Fig. 5(c)). Large-sectional combined images of the BCC specimen and zoomed combined images at 3 regions of interest (ROIs) are shown in Fig. 5(d, e) and (f-h). The large-sectional combined images were generated by mosaicking 16×8 images acquired via sample translation in a raster pattern. FOV of the mosaic image was approximately 5 mm x 3 mm and the imaging took approximately 10 min. Combined images were presented in the TPF/SHG and RC channels. The mosaic combined image showed dense cellular structures in the upper left and entire mid-right sides and ECM rich structures on the lower left side in the TPF/SHG channel, and meso-scale structures of BCC nests and surrounding fibers in the RC channel.

Moxifloxacin TP images identified two different regions: one consisting of high-density cells and no ECM, and the other consisting of mostly ECM. On the other hand, RC images did not distinguish the two regions clearly. Three regions of interest (ROIs) were selected in the mosaic image for detail analysis. One inside the cancer region (ROI-1), one outside the cancer region (ROI-2), and one on the border (ROI-3) were selected as marked in the mosaic image. Zoomed images of the three ROIs showed different microstructures. The one inside the cancer (ROI-1) showed cancer cell nests mostly. Cell clusters in the nests were shown in the TPF channel with moxifloxacin labeling, and there was small portion of collagen in between cancer cell nests. Individual cells were not resolvable due to little intensity difference on the cell boundaries, but some cells could be identified with slight contrast among the cell nucleus and cytoplasm. In the RC channel, morphologies of cancer cell nests were visible by expressing relatively high reflection in the nest compared to in between the nests. Some cells inside the nests were resolvable with the variation of reflection intensities. There was a fibrous structure on the lower left corner of the image, and the fibrous structure was correlated with the collagen structure shown in the TPF/SHG channel. In ROI-2, the zoomed combined image showed ECM structures mostly in the TPF/SHG channel and fibrous structures in the RC channel. The TP image showed collagen and elastin of the ECM and some scattered cells. Elastin fibers appeared clearly, because intrinsic AF levels were strong enough. The scattered cells could not be identified exactly whether they were stromal cells, inflammatory cells, or cancer cells. Because ROI-2 had intact ECM and BCC tends not to invade as single cells, ROI-2 was considered as the normal region. The RC image showed mostly fibrous structures which were different from BCC nests. In ROI-3, the zoomed combined image showed the boundary between BCC nests and ECM rich regions. Both the BCC nests and surrounding ECM were shown on the upper and lower sides of the image, respectively in the TPF/SHG channel, and round nest structures and fibrous structures were shown on the upper and lower sides in the RC channels, respectively. The TP image showed densely scattered cells on the boundary and these could be immune cells. Other than the densely scattered cells, the lower side of ROI-3 was similar to ROI-2. The RC image showed nest structures on the upper side and fibrous structures on the lower side. Although normal skin tissue was shown in small portion of the specimen, moxifloxacin TP and RC images provided information of microstructures in the

Biomedical Optics EXPRESS

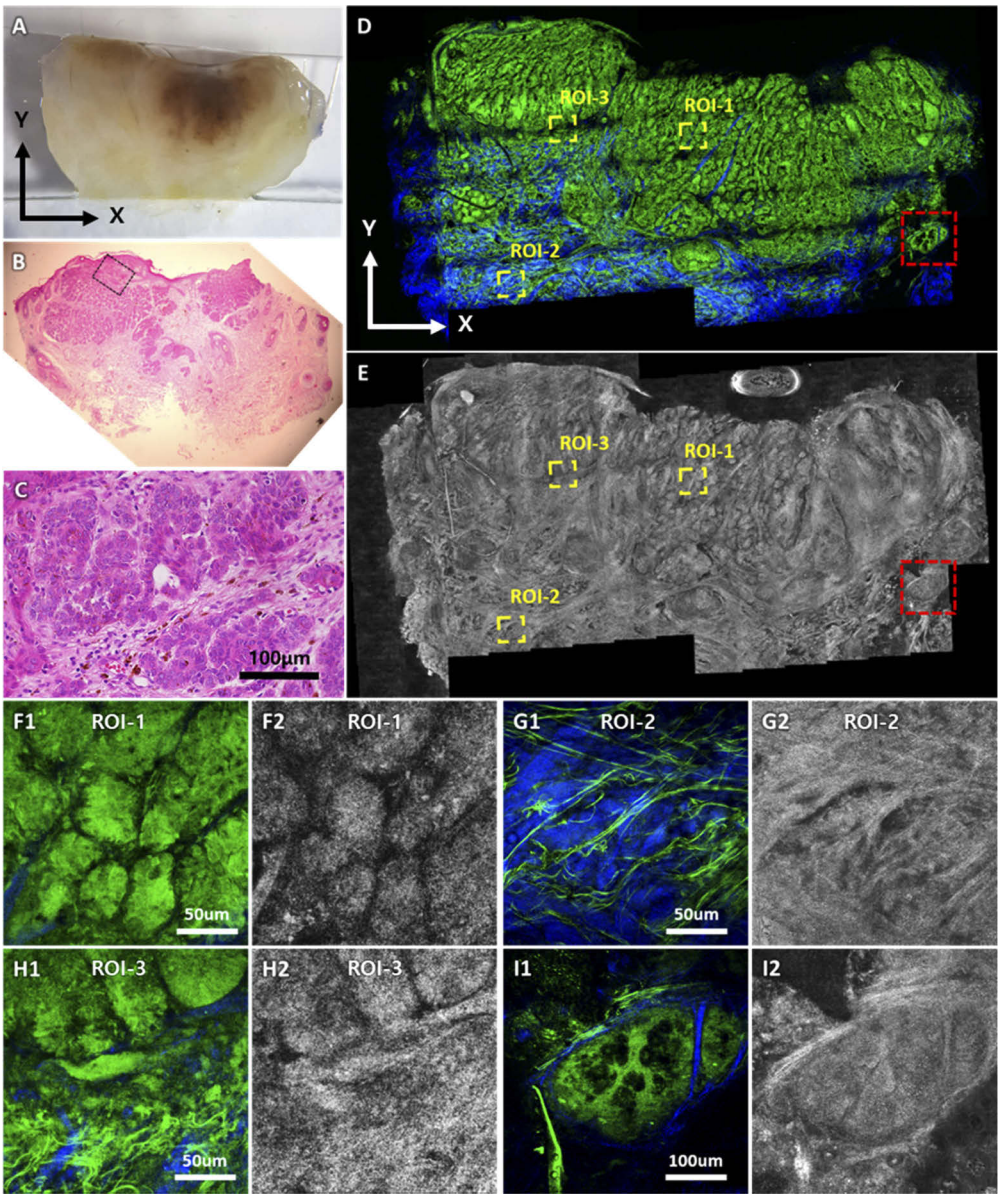

Fig. 5. A bright-field image, histological images, and moxifloxacin TP and RC images (5 mm x 3 mm in size) of a human BCC specimen, *ex vivo*. (A): a bright-field image of the BCC specimen. (B, C) hematoxylin and eosin (H&E) stained histological images in two different scales. A cell-rich region in (B) was marked with a black dash lined square and a zoomed image is shown in (C). (D, E) Large-sectional mosaic moxifloxacin TP and RC images of the human BCC just below the surface. The moxifloxacin TP image was color-coded in green and blue scales for moxifloxacin fluorescence and SHG, respectively. The RC image was color-coded in gray scale. 3 region-of-interests (ROIs) are marked with yellow dash lined squares and zoomed moxifloxacin TP and RC images of the 3 ROIs are shown in (F1, 2 – H1, 2). (F1, 2): moxifloxacin TP and RC images of ROI-1 which is abundant in cancer cells (Visualization 3). (G1-2): moxifloxacin TP and RC images of ROI-2, which is abundant in ECM (Visualization 4). (H1-2): moxifloxacin TP and RC images of ROI-3, which is on the boundary of the cell and ECM rich regions (Visualization 5). Marked with red dash lined squares are zoomed moxifloxacin TP and RC images (I1, 2). (I1, 2): moxifloxacin TP and RC images of sebaceous gland.

Biomedical Optics EXPRESS

skin dermis. There was a cell cluster structure with distinct morphology on the right lower side of the large sectional TP image, marked with a red dashed line rectangle (Fig. 5(i)). The cellular structure was considered as a sebaceous gland, because an acinar structure like a many-lobed berry was observed in the TPF channel. The sebaceous gland was observed in the RC channel image, but its structure was not clearly differentiated from that of the cancer cell nest in the RC channel.

4. Discussion

High-speed combined RC and moxifloxacin TP microscopy was developed for non-invasive high-speed multi-modal imaging. The combined microscopy was to provide additional cell and collagen contrasts to the reflection contrast of RCM and was implemented by using a Ti-Sapphire laser. After the development and characterization, the high-speed combined microscopy was applied to *in-vivo* normal mouse skin and mouse cornea, and *ex-vivo* human skin cancer specimens. In the normal skin, both the RC and TPF channel images visualized cellular structure in the epidermis similarly but they visualized different features in the dermis. The RC channel images visualized fibrous ECM structure and vessels in the dermis. On the other hand, the TPF/SHG channel images visualized cells in the dermis with moxifloxacin labeling and additional collagen distribution in the ECM via SHG. The combined image showed the detail skin microenvironments by visualizing cells, ECM, vasculature and blood flow. Additional cell and collagen contrasts in the TPF/SHG channel images were useful for the visualization of human BCC specimens. The TPF/SHG channel images visualized BCC nests imbedded in the dermis and ECM distribution. On the other hand, RCM visualized BCC nests and fibrous ECM structures. Therefore, the additional contrasts of cell and ECM by moxifloxacin TPM were useful for the visualization of microstructures in BCC together with RCM. The same features of combined microscopy could be used for the imaging of diseased corneas. In the normal cornea, the RC channel images visualized cells in all the corneal layers owing to its transparency. The TPF/SHG channel images visualized cells in the all the corneal layers based on moxifloxacin fluorescence and collagen in the stroma based on SHG. Multiple contrasts in the combined microscopy showed epithelial cells and stromal cells in two different contrasts and provided additional collagen information in the normal cornea. Diseased corneas are not transparent due to the disruption of microstructure in both the epithelium and stroma. Multiple contrasts of the combined microscopy would be helpful for the precise detection and diagnosis in diseased corneas [28].

The level of excitation power used in this study was higher than what are used for *in vivo* label-free TPM of human skin [29–32]: 2-5 mW for imaging the superficial epidermis and 10-40 mW for imaging the deep dermis. We used a fixed excitation power of 10-12 mW to image both the epidermis and dermis of the skin due to lack of a fast power control mechanism, although less excitation power could be used for imaging the epidermis. System upgrade for precise power control is required for human applications. With the increase of scanning speed, the excitation energy deposited on each position of the sample is decreased. Therefore, there is room to increase the excitation power. The limitation of excitation power for moxifloxacin TPM needs further study by taking nonlinear photodamage effects into consideration. Moxifloxacin has been approved by the FDA for its use in normal and infected skin. However, it is unknown whether intracellular moxifloxacin concentrations for fluorescence imaging is clinically safe. For clinical trials, intracellular moxifloxacin concentrations should be determined beforehand to ensure the clinical safety.

The combined RC and moxifloxacin TP microscopy would be useful in the clinical applications of RCM, especially providing information during surgery. We anticipate moxifloxacin penetration in the human skin is more challenging than the case in the mouse skin due to the thicker epidermis owing to the more cell layers. During surgery, the skin barrier is removed and moxifloxacin is rapidly absorbed into the tissue. The combined microscopy provides additional contrasts of cells

Biomedical Optics EXPRESS

and collagen to RCM without any compromise in the imaging speed. These additional contrasts may be able to improve the sensitivity and specificity of optical microscopic examination. One disadvantage of the combined microscopy over RCM is the increased cost by using femtosecond pulse lasers as the light source. There are fixed wavelength femtosecond fiber lasers available at relatively low costs compared to the laser used in this study, and the combined microscopy can use the fixed wavelength laser without any disadvantage. The next step will be pre-clinical and clinical studies of skin cancer specimens and corneal complications, and the verification of advantages having additional contrasts in the clinical applications. The combined moxifloxacin TP and RC microscopy system can be combined with other microscopic techniques providing different contrasts to improve detection sensitivity. One example is coherent anti-Stokes Raman scattering (CARS) microscopy. CARS microscopy will be useful by providing chemical information of living tissues such as lipid and protein contents non-invasively. In particular, the additional lipid contrast will be a good addition to the combined moxifloxacin TP and RC microscopy in brain imaging for visualizing myelinated axons [33].

5. Conclusion

The combined RC and moxifloxacin TP microscopy was developed to overcome the limited contrast of RCM while keeping its advantages such as high imaging speeds and non-invasiveness. The combined microscopy could non-invasively visualize detail microstructures of tissues including cells, ECM, vasculature and blood flow by using multiple contrasts of reflectance, fluorescence and SHG. The combined microscopy might be useful for clinical applications of RCM by providing multi-contrast information.

Funding

Ministry of Science, ICT and Future Planning (NRF-2017M3C7A 1044964); National Research Foundation of Korea (2017R1A2A1A18070960).

Acknowledgments

This research was supported in part by Korea-Sweden Research Cooperation Program (No. NRF-2017R1A2A1A18070960) of the National Research Foundation (NRF) funded by the Korean Government and Brain Research Program (NRF-2017M3C7A 1044964) funded by the Ministry of Science & ICT & Future Planning of the Korean Government through the NRF of Korea.

Disclosures

The authors declare no conflicts of interest.

References

1. M. Rajadhyaksha, M. Grossman, D. Esterowitz, and R. H. Webb, "*In-Vivo* Confocal Scanning Laser Microscopy of Human Skin - Melanin Provides Strong Contrast," J. Invest. Dermatol. **104**(6), 946–952 (1995).
2. Y. G. Patel, K. S. Nehal, I. Aranda, Y. B. Li, A. C. Halpern, and M. Rajadhyaksha, "Confocal reflectance mosaicing of basal cell carcinomas in Mohs surgical skin excisions," J. Biomed. Opt. **12**(3), 034027 (2007).
3. S. Ziefle, D. Schule, H. Breuninger, W. Schippert, and M. Moehrle, "Confocal Laser Scanning Microscopy vs 3-Dimensional Histologic Imaging in Basal Cell Carcinoma," Arch. Dermatol. **146**(8), 843–847 (2010).
4. Z. Y. Pan, J. R. Lin, T. T. Cheng, J. Q. Wu, and W. Y. Wu, "*In Vivo* Reflectance Confocal Microscopy of Basal Cell Carcinoma: Feasibility of Preoperative Mapping of Cancer Margins," Dermatol. Surg. **38**(12), 1945–1950 (2012).
5. S. Gonzalez and Z. Tannous, "Real-time, *in vivo* confocal reflectance microscopy of basal cell carcinoma," J. Am. Acad. Dermatol. **47**(6), 869–874 (2002).
6. E. Brasnu, T. Bourcier, B. Dupas, S. Degorge, T. Rodallec, L. Laroche, V. Borderie, and C. Baudouin, "*In vivo* confocal microscopy in fungal keratitis," Br. J. Ophthalmol. **91**(5), 588–591 (2007).
7. E. C. Ledbetter, N. L. Irby, and S. G. Kim, "*In vivo* confocal microscopy of equine fungal keratitis," Vet. Ophthalmol. **14**(1), 1–9 (2011).

Biomedical Optics EXPRESS

8. M. Y. Al-Arashi, E. Salomatina, and A. N. Yaroslavsky, "Multimodal confocal microscopy for diagnosing non-melanoma skin cancers," Lasers Surg. Med. **39**(9), 696–705 (2007).
9. Y. Y. Li, S. Gonzalez, T. H. Terwey, J. Wolchok, Y. B. Li, L. Aranda, R. Toledo-Crow, and A. C. Halpern, "Dual mode reflectance and fluorescence confocal laser scanning microscopy for *in vivo* imaging melanoma progression in murine skin," J. Invest. Dermatol. **125**(4), 798–804 (2005).
10. A. L. Carlson, L. G. Coghlan, A. M. Gillenwater, and R. R. Richards-Kortum, "Dual-mode reflectance and fluorescence near-video-rate confocal microscope for architectural, morphological and molecular imaging of tissue," J. Microsc. **228**(1), 11–24 (2007).
11. M. Hughes, V. Simaiaki, T. P. Chang, and G. Z. Yang, "Dual mode fibre bundle confocal endomicroscopy: combining reflectance and fluorescence imaging," Advanced Microscopy Techniques Iii **8797**(2013).
12. B. Masters and P. So, "Confocal microscopy and multi-photon excitation microscopy of human skin *in vivo*," Opt. Express **8**(1), 2–10 (2001).
13. W. L. Chen, Y. Sun, W. Lo, H. Y. Tan, and C. Y. Dong, "Combination of multiphoton and reflective confocal imaging of cornea," Microsc. Res. Tech. **71**(2), 83–85 (2008).
14. S. M. Zhuo, J. X. Chen, X. S. Jiang, K. C. Lu, and S. S. Xie, "Imaging rat esophagus using combination of reflectance confocal and multiphoton microscopy," Laser Phys. Lett. **5**(8), 614–618 (2008).
15. W. L. Chen, C. K. Chou, M. G. Lin, Y. F. Chen, S. H. Jee, H. Y. Tan, T. H. Tsai, K. H. Kim, D. Kim, P. T. So, S. J. Lin, and C. Y. Dong, "Single-wavelength reflected confocal and multiphoton microscopy for tissue imaging," J. Biomed. Opt. **14**(5), 054026 (2009).
16. C. A. Patil, C. L. Arrasmith, M. A. Mackanos, D. L. Dickensheets, and A. Mahadevan-Jansen, "A handheld laser scanning confocal reflectance imaging-confocal Raman microspectroscopy system," Biomed. Opt. Express **3**(3), 488–502 (2012).
17. Z. G. Wu, L. W. Jiang, W. B. Wang, J. H. Zhao, H. Lui, and H. S. Zeng, "Precise *in vivo* tissue micro-Raman spectroscopy with simultaneous reflectance confocal microscopy monitoring using a single laser," Opt. Lett. **44**(6), 1383–1386 (2019).
18. W. Denk, J. H. Strickler, and W. W. Webb, "Two-photon laser scanning fluorescence microscopy," Science **248**(4951), 73–76 (1990).
19. T. Wang, W. H. Jang, S. Lee, C. J. Yoon, J. H. Lee, B. Kim, S. Hwang, C. P. Hong, Y. Yoon, G. Lee, V. H. Le, S. Bok, G. O. Ahn, J. Lee, Y. S. Gho, E. Chung, S. Kim, M. H. Jang, S. J. Myung, M. J. Kim, P. T. So, and K. H. Kim, "Moxifloxacin: Clinically compatible contrast agent for multiphoton imaging," Sci. Rep. **6**(1), 27142 (2016).
20. W. H. Jang, Y. Yoon, W. Kim, S. Kwon, S. Lee, D. Song, J. W. Choi, and K. H. Kim, "Visualization of laser tattoo removal treatment effects in a mouse model by two-photon microscopy," Biomed. Opt. Express **8**(8), 3735–3748 (2017).
21. J. H. Lee, V. H. Le, S. Lee, J. H. Park, J. A. Lee, H. Tchah, S. Kim, M. J. Kim, and K. H. Kim, "Two-photon microscopy of fungal keratitis-affected rabbit cornea *ex vivo* using moxifloxacin as a labeling agent," Exp. Eye Res. **174**, 51–58 (2018).
22. S. Lee, J. H. Lee, T. Wang, W. H. Jang, Y. Yoon, B. Kim, Y. W. Jun, M. J. Kim, and K. H. Kim, "Three-photon tissue imaging using moxifloxacin," Sci. Rep. **8**(1), 9415 (2018).
23. H. Chang, W. H. Jang, S. Lee, B. Kim, M. J. Kim, W. O. Kim, Y. W. Ryoo, B. H. Oh, and K. H. Kim, "Moxifloxacin Labeling-Based Multiphoton Microscopy of Skin Cancers in Asians," Lasers Surg Med (2019).
24. K. Dabov, A. Foi, V. Katkovnik, and K. Egiazarian, "Image denoising by sparse 3-D transform-domain collaborative filtering," IEEE Trans. on Image Process. **16**(8), 2080–2095 (2007).
25. W. H. Jang, S. Kwon, S. Shim, W. S. Jang, J. K. Myung, S. Yang, S. Park, and K. H. Kim, "Comparison between reflectance confocal microscopy and 2-photon microscopy in early detection of cutaneous radiation injury in a mouse model *in vivo*," J. Biophotonics **11**(10), e201700337 (2018).
26. S. Yousefi, J. Qin, Z. W. Zhi, and R. K. K. Wang, "Label-free optical lymphangiography: development of an automatic segmentation method applied to optical coherence tomography to visualize lymphatic vessels using Hessian filters," J. Biomed. Opt. **18**(8), 086004 (2013).
27. S. Levet, D. Ciais, G. Merdzhanova, C. Mallet, T. A. Zimmers, S. Lee, F. P. Navarro, I. Texier, J. Feige, S. Bailly, and D. Vittet, "Bone morphogenetic protein 9 (BMP9) controls lymphatic vessel maturation and valve formation," Blood **122**(4), 598–607 (2013).
28. J. H. Lee, S. Lee, C. J. Yoon, J. H. Park, H. Tchah, M. J. Kim, and K. H. Kim, "Comparison of reflectance confocal microscopy and two-photon second harmonic generation microscopy in fungal keratitis rabbit model *ex vivo*," Biomed. Opt. Express **7**(2), 677–687 (2016).
29. M. Balu, C. B. Zachary, R. M. Harris, T. B. Krasieva, K. Konig, B. J. Tromberg, and K. M. Kelly, "*In Vivo* Multiphoton Microscopy of Basal Cell Carcinoma," JAMA Dermatol **151**(10), 1068–1074 (2015).
30. G. Lentsch, M. Balu, J. Williams, S. Lee, R. M. Harris, K. Konig, A. Ganesan, B. J. Tromberg, N. Nair, U. Santhanam, and M. Misra, "*In vivo* multiphoton microscopy of melasma," Pigm. Cell Melanoma Res. **32**(3), 403–411 (2019).
31. M. Balu, G. Lentsch, D. Z. Korta, K. Konig, K. M. Kelly, B. J. Tromberg, and C. B. Zachary, "*In vivo* multiphoton-microscopy of picosecond-laser-induced optical breakdown in human skin," Lasers Surg. Med. **49**(6), 555–562 (2017).

Biomedical Optics EXPRESS

32. R. Cicchi, D. Kapsokalyvas, V. De Giorgi, V. Maio, A. Van Wiechen, D. Massi, T. Lotti, and F. S. Pavone, "Scoring of collagen organization in healthy and diseased human dermis by multiphoton microscopy," J. Biophoton. **3**(1-2), 34–43 (2009).
33. V. H. Le, S. W. Yoo, Y. Yoon, T. Wang, B. Kim, S. Lee, K. H. Lee, K. H. Kim, and E. Chung, "Brain tumor delineation enhanced by moxifloxacin-based two-photon/CARS combined microscopy," Biomed. Opt. Express **8**(4), 2148–2161 (2017).